

Mass-Temperature Relation of Galaxy Clusters: A Theoretical Study

Niayesh Afshordi¹ and Renyue Cen²

Received _____; accepted _____

¹Princeton University Observatory, Princeton University, Princeton, NJ 08544;
afshordi@astro.princeton.edu

²Princeton University Observatory, Princeton University, Princeton, NJ 08544;
cen@astro.princeton.edu

A B S T R A C T

Combining conservation of energy throughout nearly-spherical collapse of galaxy clusters with the virial theorem, we derive the mass-temperature relation for X-ray clusters of galaxies $T = C M^{2/3}$. The normalization factor C and the scatter of the relation are determined. We are also able to reproduce the recently observed break in the $M-T$ relation at $T = 3 \text{ keV}$, based on the scatter in the underlying density field for a low density CDM cosmology. Finally, by combining observational data of high redshift clusters with our theoretical formalism, we find a semi-empirical temperature-mass relation which is expected to hold at redshifts up to unity with less than 5% systematic error.

Subject headings: Cosmology: theory { large-scale structure of universe { galaxies: clusters { galaxies: halos

1. Introduction

The abundance of clusters of galaxies provides one of the strongest constraints on cosmological models (Peebles, Daly, & Juszkiewicz 1989; Bahcall & Cen 1992; White, Efstathiou, & Frenk 1993; Viana & Liddle 1996; Eke, Cole, & Frenk 1996; Oukbir, Bartlett, & Blanchard 1997; Bahcall, Fan, & Cen 1997; Pen 1998; Henry 2000) with an uncertainty on the amplitude of density fluctuations of about 10% on $10h^{-1}Mpc$ scale. Theoretically it is often desirable to translate the mass of a cluster, that is predicted by either analytic theories such as Press-Schechter (1974) theory or N-body simulations, to the temperature of the cluster, which is directly observed. Simple arguments based on virialization density suggest that $T \propto M^{2/3}$, where T is the temperature of a cluster within a certain radius (e.g., the virial radius) and M is the mass within the same radius. However, the proportionality coefficient has not been self-consistently determined from first principles, although numerical simulations have frequently been used to calibrate the relation (e.g., Evrard, Metzler, & Navarro 1996, hereafter EMN; Bryan & Norman 1998; Thomas et al. 2001).

It is noted that the results from different observational methods of mass measurements are not consistent with one another and with the simulation results (e.g., Hörner, Mushotzky, & Scharf 1999, hereafter HMS; Neumann, & Amaud 1999; Nevalainen, Markevitch, & Forman 2000, Finoguenov, Reiprich, & Böhringer 2001, hereafter FRB). In general, X-ray mass estimates are about 80% lower than the predictions of hydro-simulations. Fig 1 compares X-ray cluster observational data with best fit line to EMN simulation results (FRB). On the other hand, mass estimates from galaxy velocity dispersion seem to be consistent with simulation results (HMS). The error in the gravitational lensing mass measurements is still too big to distinguish between these two (Hjorth, Oukbir & van Kampen 1998).

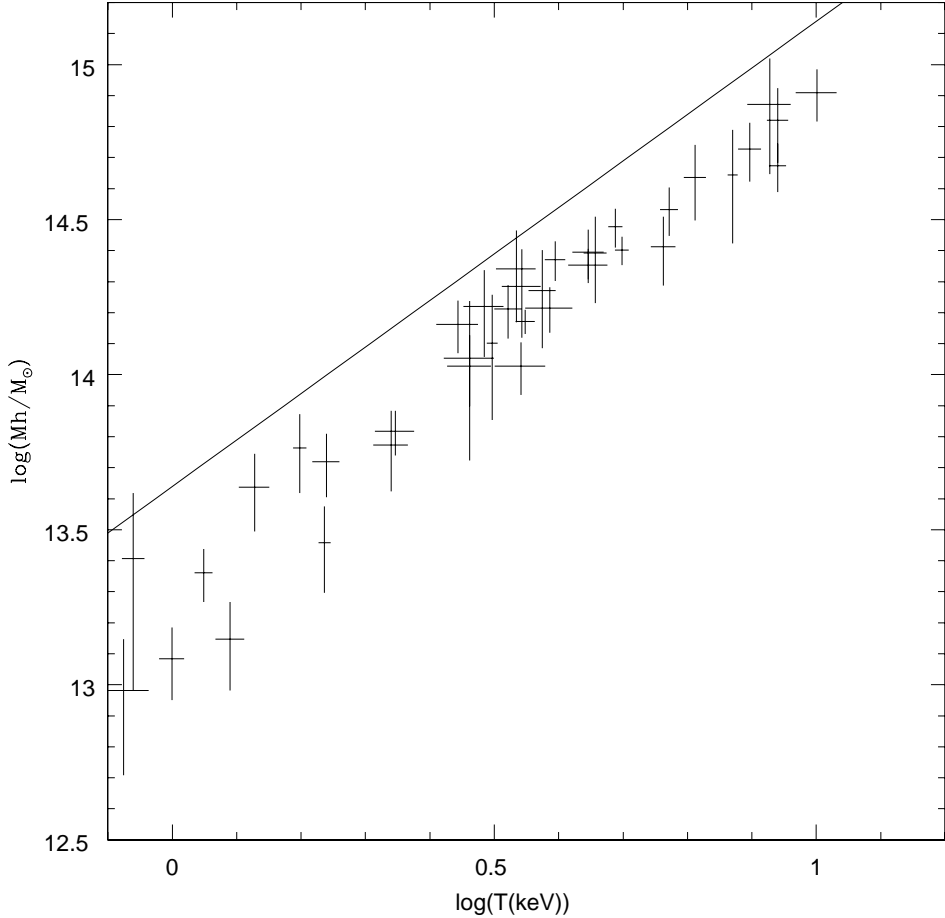


Fig. 1. | Observational mass-temperature data based on temperatures of X-ray clusters (crosses with 1 error bars) vs. the best fit line to EMN simulation results (FRB).

Another recent observational finding is the possible existence of a break in the $T \propto M$ relation. By use of resolved temperature profile of X-ray clusters observed by ASCA, FRB have investigated $T \propto M$ relation in the low-mass end and find that $M \propto T^{-2}$, compared to $M \propto T^{-3/2}$ at the high mass end. Suggestions have been made to explain this behavior by attributing it the effect of formation redshift (FRB), cooling (Muawwad et al. 2001) and heating (Bialek, Evrard & Mohn 2000) processes.

In this paper we use conservation of energy for an almost spherically collapsing region to derive the M-T relation. In x2 we find the initial and final energy of the cluster. x3 constrains various factors which enter the normalization of M-T relation, via statistical methods, simulation and observational input. x4 considers predictions of our model and comparison with observational and simulation results. In x5, we discuss the limitations of our approach and justify some of the approximations. x6 concludes the paper

2. Conservation of Energy

2.1. Initial Kinetic and Potential Energy of a Proto-Cluster

We begin by deriving the kinetic energy of the proto-cluster. We can write velocity as a function of gravitational potential ϕ_i (e.g. Padmanabhan 1993):

$$v = H_i x - \frac{2}{3H_i} r_i; \quad (1)$$

at the initial time in the linear regime, where H_i is the Hubble constant at the initial time. There is a small dependence on the initial density parameter Ω_i in equation (1) which we ignore since initially it is very close to unity and the difference will be in second order terms that we ignore for the proto-cluster. Then the kinetic energy is given by:

$$K_i = \frac{1}{2} \int_{-r_i}^{r_i} v^2 d^3x = \frac{1}{2} \int_{-r_i}^{r_i} (1 + \Omega_i) H_i x - \frac{2}{3H_i} r_i d^3x; \quad (2)$$

Keeping the terms up to the linear order we obtain

$$K_i = \frac{1}{2} \int_{-r_i}^{r_i} (H_i^2 x^2 + \frac{2}{3} r_i^2 \Omega_i x^2 - \frac{4}{3} x r_i) d^3x; \quad (3)$$

In deriving equation (3), we have used the Poisson equation:

$$r_i^2 \Omega_i = 4 \pi G \rho_i; \quad (4)$$

to substitute for ρ_i , where ρ_i is the initial mean density of the universe. For equation (3) we then use Gauss theorem to make the third term similar to the second, at the expense of a surface term :

$$K_i = \frac{1}{2} \int_i^Z (H_i^2 x^2 + \frac{4}{3} x^2 r_i^2) d^3 x - \frac{1}{3} \int_i^I x^2 r_i da; \quad (5)$$

Assuming that the deviations from spherical symmetry is not important at the boundary of the proto-cluster, we find r_i in the second term in equation (5) as a function of ρ_i :

$$r_i = \frac{G M}{R_i^2} = \frac{G \rho_i}{R_i^2} \int_i^Z d^3 x; \quad (6)$$

where G is the gravitational constant and R_i is the boundary radius of the initial proto-cluster, which leads to

$$K_i = \frac{4 G \rho_i^2}{3} \int_i^Z [(1 + 2 \rho_i) x^2 - R_i^2] d^3 x; \quad (7)$$

where we have used equation (4) to substitute back for ρ_i and also the definition of $\rho_i = 8 \pi G / (3H_i^2)$.

Let us now find an expression for the gravitational potential energy of the proto-cluster. Using its definition we have

$$U_i = \frac{G \rho_i^2}{2} \int_i^Z \frac{(1 + 2 \rho_i(x_1))(1 + 2 \rho_i(x_2))}{|x_1 - x_2|} d^3 x_1 d^3 x_2; \quad (8)$$

Keeping the terms to the first order and using the symmetry under interchange of x_1 and x_2 , we arrive at

$$U_i = \frac{G \rho_i^2}{2} \int_i^Z (1 + 2 \rho_i(x_1)) d^3 x_1 \int_i^Z \frac{d^3 x_2}{|x_1 - x_2|}; \quad (9)$$

which, taking the second integral in a spherical volume, gives

$$U_i = \frac{4 G \rho_i^2}{3} \int_i^Z (1 + 2 \rho_i) \left(\frac{3R_i^2 - x^2}{4} \right) d^3 x; \quad (10)$$

Adding equations 7 and 10 gives the total initial energy:

$$E_i = \frac{4 G \rho_i^2}{3} \left[\frac{4}{5} (1 + 2 \rho_i) R_i^5 - \frac{5}{2} \int_i^Z \rho_i(x) (R_i^2 - x^2) d^3 x \right]; \quad (11)$$

to the first order. Defining \mathbf{x} , $\tilde{\mathbf{v}}_i$ and B as:

$$\mathbf{x} = \frac{\mathbf{x}}{R_i}; \tilde{\mathbf{v}}_i = \mathbf{v}_i + \frac{3}{5}(\mathbf{v}_i - \mathbf{v})_i; B = \int_0^{R_i} \tilde{\mathbf{v}}_i(\mathbf{x}) (1 - \mathbf{x}^2) d^3 \mathbf{x}; \quad (12)$$

equation (11) is simplified:

$$E_i = \frac{10}{3} G \int_0^{R_i} \tilde{\mathbf{v}}_i^2 B : \quad (13)$$

The integral in the definition of B is in fact a three dimensional integral and the limits denote that the integration domain is the unit sphere. Note that $\tilde{\mathbf{v}}_i$ can be considered as the density perturbation to a flat (i.e. $\Omega_{\text{tot}} = 1$) universe for which energy vanishes. Another aspect of this statement is that both terms in the definition of $\tilde{\mathbf{v}}_i$ scale as a in the early (matter dominated) universe and so does $\tilde{\mathbf{v}}_i$ itself. For a flat universe the first term dominates at high redshift since the second term scales as a^3 .

2.2. Energy of a Virialized Cluster

According to the virial theorem, the sum of the total energy E_f of a virialized cluster and its kinetic energy K_f vanishes. However, non-vanishing pressure at the boundary of the cluster can significantly modify the virial relation. Integrating the equation of hydrostatic equilibrium, we have

$$K_f + E_f = 3P_{\text{ext}}V; \quad (14)$$

where P_{ext} is the pressure on the outer boundary of virialized region (i.e. virial radius) and V is the volume. For now we assume that the surface term is related to the total potential energy U_f by

$$3P_{\text{ext}}V = -U_f: \quad (15)$$

We will consider the coefficient and its possible mass dependence in section 3.4. For a system of fully ionized gas plus dark matter, the virial relation (14) with equation (15) leads to

$$\left(\frac{1}{2} + \frac{1}{M_{\text{DM}}}\right)E_f = K_f = \frac{3}{2}M_{\text{DM}} \frac{v^2}{V} + \frac{3M_{\text{gas}}kT}{2m_p}; \quad (16)$$

where v is the mass-weighted mean one-dimensional velocity dispersion of dark matter particles, M_{DM} is the total dark matter mass, k is the Boltzmann constant, $\gamma = 0.59$ is the mean molecular weight and m_p is the proton mass. Assuming that the ratio of gas to dark matter mass in the cluster is the same as that of the universe as a whole and f is the fraction of the baryonic matter in the hot gas, we get

$$K_f = \frac{3 \tilde{\rho}_{\text{spec}} M k T}{2 m_p} [1 + (f \tilde{\rho}_{\text{spec}}^{-1} - 1) \frac{b}{m}] : \quad (17)$$

with $\tilde{\rho}_{\text{spec}}^2 = (kT = m_p)$. Hydrodynamic simulations indicate that $\tilde{\rho}_{\text{spec}} \approx 1$. For simplicity we define $\tilde{\rho}_{\text{spec}}$ as

$$\tilde{\rho}_{\text{spec}} = \tilde{\rho}_{\text{spec}} [1 + (f \tilde{\rho}_{\text{spec}}^{-1} - 1) \frac{b}{m}] : \quad (18)$$

So equation (16) reduces to:

$$K_f = \frac{3 \tilde{\rho}_{\text{spec}} M k T}{2 m_p} : \quad (19)$$

Assuming energy conservation (i.e., $E_i = E_f$) and combining this result with equations (13, 16) lead to the temperature as a function of initial density distribution:

$$kT = \frac{5 m_p}{8 \tilde{\rho}_{\text{spec}}} \left(\frac{1 + b}{1} \right) H_i^2 R_i^2 B : \quad (20)$$

In the next subsection x2.3 we will find an expression for $H_i^2 R_i^2$ in terms of cluster mass M and the initial density fluctuation spectrum.

2.3. Initialization Time

Defining e as the energy of a test particle with unit mass, which is at the boundary of the cluster R_i of mass M initially:

$$e = \frac{v_i^2}{2} - \frac{G M}{R_i} : \quad (21)$$

{ 9 }

The collapse time t can be written as

$$t = \frac{2 GM}{(2e)^{\frac{3}{2}}} : \quad (22)$$

Following the top-hat model, we assume that the collapse time of the particle is approximately the same as the time necessary for the particle to be virialized. Choosing t to be the time of observation and assuming the mass M , interior to the test particle is virialized at t , and by combining equations (1, 6, 22), we find e as function of initial density distribution and relate it to the collapse time:

$$2e = \frac{5}{4} H_i^2 R_i^2 \int_0^{Z_i} \tilde{\rho}_i(x) d^3x = \left(\frac{2 GM}{t} \right)^{\frac{2}{3}} : \quad (23)$$

Using $M = \frac{4}{3} \pi R_i^3 \rho_i$ and the Friedmann equations we obtain

$$A = \int_0^{Z_i} \tilde{\rho}_i(x) d^3x = \frac{2}{5} \left(\frac{3^4}{t^2 G} \right)^{\frac{1}{3}} : \quad (24)$$

2.4. M-T Relation

Combining equations (20) and (13,24), we arrive at the cluster temperature-mass relation:

$$kT = \left(\frac{m_p}{2 \tilde{\rho}_{\text{spec}}} \right) \left(\frac{1 +}{1} \right) \left(\frac{2 GM}{t} \right)^{\frac{2}{3}} \left(\frac{B}{A} \right) : \quad (25)$$

Notice that although B and A are both functions of the initial moment t_i , since both are proportional to the scale factor a , the ratio is a constant; the derived T-M relation (equation 25) does not depend on the adopted initial time, as expected. As a specific example, in the spherical top-hat model in which the density contrast is assumed to be constant, this ratio B/A is $\frac{2}{5}$. Let us gather all the unknown dimensionless factors in Ω :

$$\Omega = \left(\frac{\tilde{\rho}_{\text{spec}}}{0.9} \right)^{\frac{1}{3}} \left(\frac{1 +}{1} \right) \left(\frac{B}{A} \right) (H t)^{\frac{2}{3}} : \quad (26)$$

Then, inserting in the numerical values, equation (25) reduces to:

$$kT = (6.62 \text{ keV}) \mathcal{Q} \left(\frac{M}{10^{15} h^{-1} M_{\odot}} \right)^{2/3}; \quad (27)$$

or equivalently:

$$M = 5.88 \times 10^{13} \mathcal{Q}^{1.5} \left(\frac{kT}{1 \text{ keV}} \right)^{1.5} h^{-1} M_{\odot} \quad (28)$$

where $H = 100h \text{ km/s/Mpc}$ is the Hubble constant. This result can be compared with the EMN simulation results:

$$M_{200} = (4.42 \pm 0.56) \times 10^{13} \left(\frac{kT}{1 \text{ keV}} \right)^{1.5} h^{-1} M_{\odot} \quad (29)$$

To convert the M_{500} masses of EMN to M_{200} we have used the observed scaling of the mass with density contrast $M_{500} / M_{200}^{0.266}$ (HMS), which is consistent with the NFW profile (Navarro, Frenk, & White 1997) for simulated dark matter halos as well as observations (e.g., Tyson, Kochanski, & dell'Antonio 1998), in the relevant range of radius.

3. Numerical Factors, Scatter and Uncertainties

In this section we try to use different analytical methods as well as the results of dark matter simulations and observed gas properties, available in the literature, to constrain the numerical factors which appear in \mathcal{Q} (equation 26).

3.1. $\mathcal{Q}_{\text{spec}}$ and the gas fraction

So far we have made no particular assumption about the gas dynamics or its history,³ and so we are going to rely on the available observational results to constrain gas properties.

³With the exception of any heating/cooling of the gas being negligible with respect to the gravitational energy of the cluster.

ζ_{spec} is defined as the ratio of kinetic energy per unit mass of dark matter to the thermal energy of gas particles. This ratio is typically of the order of unity, though different observational and theoretical methods lead to different values.

The hydrodynamic simulation results usually point to a larger value of ζ_{spec} . For example, Thomas et al. (2001) find $\zeta_{\text{spec}} = 0.94 \pm 0.03$. On the other hand, observational data point to a slightly lower value of ζ_{spec} . Observationally there is yet no direct way of accurately measuring the velocity dispersion of dark matter particles in the cluster and one is required to assume that the velocity distribution of galaxies follows that of dark matter or adopt a velocity bias. Under the assumption of no velocity bias Girardi et al. 1998 find it to be 0.88 ± 0.04 . Girardi et al. 2000 study ζ_{spec} for a sample of high redshift clusters and do not find any evidence for redshift dependence. From the theoretical point of view, the actual value of ζ_{spec} might be substantially different from the observed number, because both the velocity and density of galaxies do not necessarily follow those of the dark matter, which could have resulted in some non-negligible selection effects. Unknown sources of heating such as due to gravitational energy on small scales which is often substantially underestimated in simulations due to limited resolutions or baryonic processes like supernova feedback may affect the value of ζ_{spec} as well.

Hydrodynamic simulations show that only a small fraction of the baryons contribute to galaxy formation in large clusters (e.g., Blanton et al. 2000) and so f is close to one. Observationally we quote Bryan (2000) who compiled different observations for the cluster mass fraction in gas and galactic component with

$$f = 1 - 0.26(T=10 \text{ keV})^{-0.35}; \quad (30)$$

albeit with a large scatter in the relation. Inserting equation (30) into equation (18), we see that the correction to $\zeta_{\text{spec}} = 0.9$ is less than 5% for all of feasible cosmological models which are dominated by non-baryonic dark matter. In what follows, unless mentioned otherwise,

we adopt the value $\tilde{\gamma}_{\text{spec}} = 0.9$ and absorb any correction into the overall normalization of the $T \rightarrow M$ relation.

3.2. $B = A$: Single Central Peak Approximation and Freeze-Out time

In the original top-hat approximation (Gunn & Gott 1972) which has been extensively used in the literature, the initial density distribution is assumed to be constant inside R_i , which leads to $B = A = 2 = 5$. Here we consider the general case with an arbitrary density profile of a single density peak. But before going further, let us separate out the term due to space curvature in the definition of $B = A$. Using the definitions of B and A in equations (12) and (24), and Friedmann equations to insert for γ_i in terms of the present day cosmological parameters, we get:

$$\frac{B}{A} = \frac{b}{a} + \left(\frac{b}{a} - \frac{2}{5} \right) \left(1 - \frac{m}{m} \right) \left(\frac{H t}{m} \right)^{\frac{2}{3}}; \quad (31)$$

where m and m are the density parameters due to non-relativistic matter and cosmological constant, respectively, at the time of observation, a and b are⁴ the same as A and B with $\tilde{\gamma}_i$ replaced by γ_i in their definitions, equations (24) and (12).

Assuming that the initial density profile has a single, spherically symmetric peak and assuming a power law for the initial linear correlation function at the cluster scale, we can replace $\gamma(x)$ by $\frac{\gamma(x)}{\gamma(0)}$,

$$\gamma(x) = \left(\frac{r_{0i}}{x} \right)^{3+n}; \quad (32)$$

where n is the index of the density power spectrum (Peebles 1981) and r_{0i} is the correlation length. This gives

$$\frac{B}{A} = \left(\frac{1}{1 - \frac{n}{2}} \right) \left[1 + \frac{(3+n)(1 - \frac{m}{m})}{5} \left(\frac{H t}{m} \right)^{\frac{2}{3}} \right]; \quad (33)$$

⁴ a should not be confused with the cosmological scale factor.

where all the quantities are evaluated at the age of the observed cluster. Note that for models of interest the physically plausible range for n is $(-3; 0)$. One can see that the second term in equation (33) is indeed proportional to $t^{\frac{2}{3}}$ and so for an open universe it dominates for large time (after curvature domination). Noting that in equation (25), the temperature is proportional to $t^{-\frac{2}{3}\frac{B}{A}}$, so, when the second term dominates, the T - M relation will no longer evolve with time. This indicates that in an open universe the cluster formation freezes out after a certain time. The presence of freeze-out time is independent of the central peak approximation since the ratio b/a only depends on the statistics of the initial fluctuations at high redshifts where there is very little dependence on cosmology. It is interesting to note that in the case $n = -3$, the ratio has no dependence on cosmology and there is no freeze-out even in low density universes, which may be stated, equivalently, that all clusters in any universe with $n = -3$ form at the time of observation.

Voit (2000) uses a different method to obtain exactly the same result. As we argue next, both treatments ignore cluster mergers.

3.3. $B = A$: Multiple Peaks and Scatter

The single peak approximation discussed in x3.2 ignores the presence of other peaks in the initial density distribution. In hierarchical structure formation models, the mass of a cluster grows with time through mergers as well as accretion. This means that multiple peaks may be present within R_i and suppress the effect of the central peak.

Assuming Gaussian statistics for initial density fluctuations, we can find the statistics of b/a . Note that using equation (24), we can fix the value A (and hence a) for a given mass and virialization time. So the problem reduces to finding the statistics of b (or B) for fixed

a. Under the assumption of a power law spectrum (see Appendix A) calculations give

$$\frac{\langle b \rangle}{a} = \frac{4(1-n)}{(n-5)(n-2)}; \quad (34)$$

with

$$b = \frac{16}{(5-n)(2-n)} \frac{2^{n-2}}{n(7-n)(n-3)} \left[\frac{n+3}{10(1-n)} \right]^{\frac{1}{2}} \left(\frac{r_{0i}}{R_i} \right)^{\frac{n+3}{2}}; \quad (35)$$

which, inserting into equation (31), yields

$$\langle \frac{B}{A} \rangle = \frac{4(1-n)}{(n-5)(n-2)} \left[1 - \frac{n(n+3)}{10(1-n)} \left(\frac{Ht}{m} \right)^{\frac{2}{3}} \right]; \quad (36)$$

$$\frac{B}{A} = (n) \left(\frac{M}{M_{0L}} \right)^{\frac{n+3}{6}} D^{-1}(t) \left(\frac{Ht}{m} \right)^{\frac{2}{3}}; \quad (37)$$

where $D(t)$ is the growth factor of linear perturbations, normalized to $(1+z)^{-1}$ for large redshift, and

$$M_{0L} = \frac{4}{3} r_{0L}^3; \quad (38)$$

$$_L(r) = \left(\frac{r_{0L}}{r} \right)^{n+3};$$

where $_L(r)$ is the linearly evolved correlation function at the present time with r_{0L} being the correlation length, and

$$(n) \frac{20}{(5-n)(2-n)} \frac{2^{n-2}}{n(7-n)(n-3)} \left[\frac{n+3}{10(1-n)} \right]^{\frac{1}{2}}; \quad (39)$$

Fig 2 shows the dependence of $B=A$ on n . The upper dotted curve shows the result of the single peak approximation (equation 33), while three lower curves show the multiple peak calculation described above (equation 36) and its 1 dispersion (equation 37). All the curves are for an Einstein-de Sitter universe and the dispersion is calculated from mass $10M_{0L}$. Numerically, for $r_{0L} = 5h^{-1}Mpc$ we have $M_{0L} = 1.4 \times 10^{14} m h^{-1} M$, resulting in $10M_{0L} = 4.3 \times 10^{14} h^{-1} M$ for $m = 0.3$. We note that $n = 3$ the density distribution is dominated by the central peak and corresponds to the top-hat case, and so two methods

give similar results. Interestingly, as n approaches zero, small peaks dominate and the distribution becomes close to homogeneous (top hat) on large scales. This implies that clusters undergo a large number of mergers for large values of n . Interestingly, in this case the ratio $B = A$ again approaches 2=5, the value for the top-hat case. We will use the multiple-peak approximation in our subsequent calculations.

It is worth mentioning that the ratio of the cosmology dependent term in the average value of $\langle B = A \rangle$ to the constant term, in the multiple-peak calculation, is small. For example, for $m = 0.3$ and $n = 1.5$, this ratio is about 0.07. This implies that the freeze-out time is large comparing to the current age of the universe for feasible open cosmological models and consequently $\langle B = A \rangle$ is determined by the spectral index of the underlying linear power spectrum n .

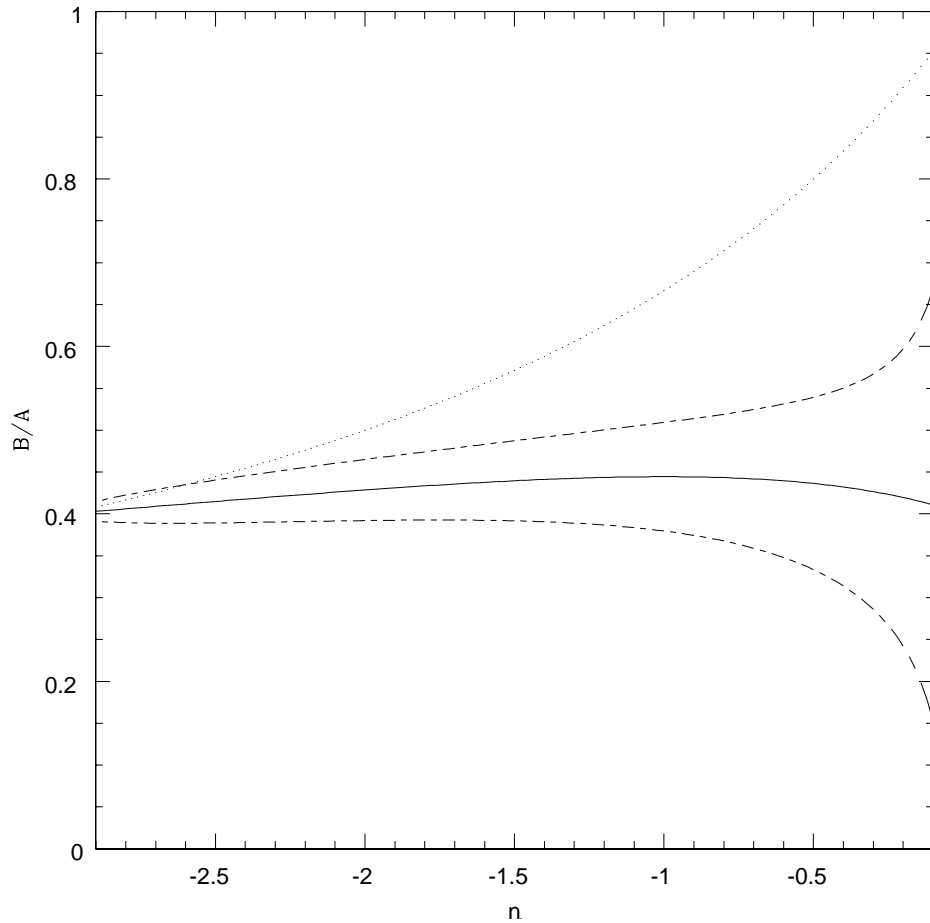


Fig. 2. | The solid curve shows B/A vs. the power index and dashed curves are its $1/\sqrt{M}$ variance for $M = 10M_{OL}$ (see the text) for an Einstein-de Sitter universe. The dotted curve is the result of single peak approximation (equation 33).

3.4. : Surface Term and its Dependence on the Nalequilibrium density profile

As discussed in x2, corrections to the virial relation due to finite surface pressure changes the M-T relation (equation 25). Voit (2000) uses NFW profile for the radial density distribution to constrain the extra factor and finds that for typical concentration parameters $c = r_{200}/r_s = 5$, $(\gamma + 1) = (\gamma - 1)$ is 2. We will investigate this correction, , for a given concentration parameter c . Let us assume that the density profile is given by:

$$\rho(r) = \rho_s f(r=r_s); \quad (40)$$

where ρ_s is a characteristic density, r_s the scale radius, and f is the density profile. For the NFW profile

$$f_{\text{NFW}}(x) = \frac{1}{x(1+x)^2}; \quad (41)$$

and for the Moore profile

$$f_M(x) = \frac{1}{x^{1.5}(1+x^{1.5})} \quad (42)$$

Moore et al. 2000, have used simulations with higher resolutions to show that the central density profile is steeper than the one already probed by low-resolution simulations such as those used by NFW .) For a given $f(x)$, the mass of the cluster is:

$$M = 4 \pi r_s^3 \rho_s g(x); g(x) = \int_0^{r_s} f(x) x^2 dx; \quad (43)$$

The gravitational energy of the cluster is given by:

$$U = \frac{1}{2} \int_0^{r_s} \frac{GM}{r} dr = 16 \pi^2 G \rho_s^2 r_s^5 \int_0^{r_s} f(x) g(x) x^2 dx; \quad (44)$$

To find the surface pressure, we integrate the equation of hydrostatic equilibrium ⁵

$$r P = g = \frac{GM}{r^3}; \quad (45)$$

⁵This is of course valid in the case of isotropic velocity dispersion profile. As an approximation, we are going to neglect any correction due to this possible anisotropy

This leads to

$$P_{\text{ext}} = 4 \pi r_s^2 \int_c^z f(x) g(x) x^2 dx; \quad (46)$$

which, by the definition of (equation 15), gives:

$$(c; f) \frac{3P_{\text{ext}}V}{U} = \frac{c^3 \int_0^{R_1} f(x) g(x) x^2 dx}{\int_0^{R_c} f(x) g(x) x dx}; \quad (47)$$

Note that $(c; f)$ is a function of both c and density profile f .

We suggest that, by using the conservation of energy, one can also constrain the concentration parameter and subsequently the surface correction for a given density profile. A typical density profile is specified by two parameters: a characteristic density r_s and scale radius r_s . If we know mass (e.g. M_{200}) and total energy of the cluster, we can fix these two parameters. The concentration parameter is then fixed by r_s and the critical density of the universe. To do this, let us re-derive the T-M relation for a known density profile. Combining equations (16) and (19) gives:

$$kT = \frac{2 m_p}{3 \tilde{M}_{\text{spec}}} \left(\frac{1 +}{1} \right) E_f; \quad (48)$$

Note that equation (48) only depends on the properties of the virialized cluster and is independent of its history. Defining y as

$$y = \frac{4E}{3M} (2 \pi G M H_0)^{2/3}; \quad (49)$$

equation (48) reduces to:

$$kT = \frac{m_p}{2 \tilde{M}_{\text{spec}}} \left(\frac{1 +}{1} \right) \left(\frac{2 \pi G M}{t_0} \right)^{2/3} [(H_0 t_0)^{2/3} y]; \quad (50)$$

Comparing this result with equation (25), we see that:

$$y = \frac{B}{A (H t)^{2/3}}; \quad (51)$$

only if the energy is conserved (i.e., assuming E_f in equation (49) is equal to E_i).

On the other hand, by combining equation (49) with equations (43), (44) and (47) and the virial theorem (14), y can be written as a function of c , for a fixed density profile f :

$$y(c; f) = \frac{\frac{1}{c} \int_0^R c f(x) g(x) dx}{3 \int_0^R g^2(x) dx}; \quad (52)$$

where we have assumed the boundary of the virialized region to be the radius at which the average density is c times the critical density of the universe (which is usually chosen to be 200), and g is a function of c and f in equation (47). Equation (52) fixes the concentration parameter c as a function of y for a fixed density profile, which in turn is determined by equation (51).

If we define $Q(c; f)$ as

$$Q(c; f) = \frac{1}{1 + \frac{1}{c}} y = \frac{1}{1 + \frac{1}{c}} \frac{B}{A (H t)^{\frac{2}{3}}}; \quad (53)$$

equation (25) can be written as:

$$kT = \frac{m_p}{2 \tilde{\rho}_{\text{spec}}} (2 \pi G H M)^{\frac{2}{3}} Q(c; f); \quad (54)$$

or in numerical terms:

$$kT = (6.62 \text{ keV}) Q(c; f) \left(\frac{M}{10^{15} h^{-1} M_{\odot}} \right)^{2/3} \quad (55)$$

for $\tilde{\rho}_{\text{spec}} = 0.9$. Note that with this choice of $\tilde{\rho}_{\text{spec}}$, the definition of Q is equivalent to that of Q in equation (26).

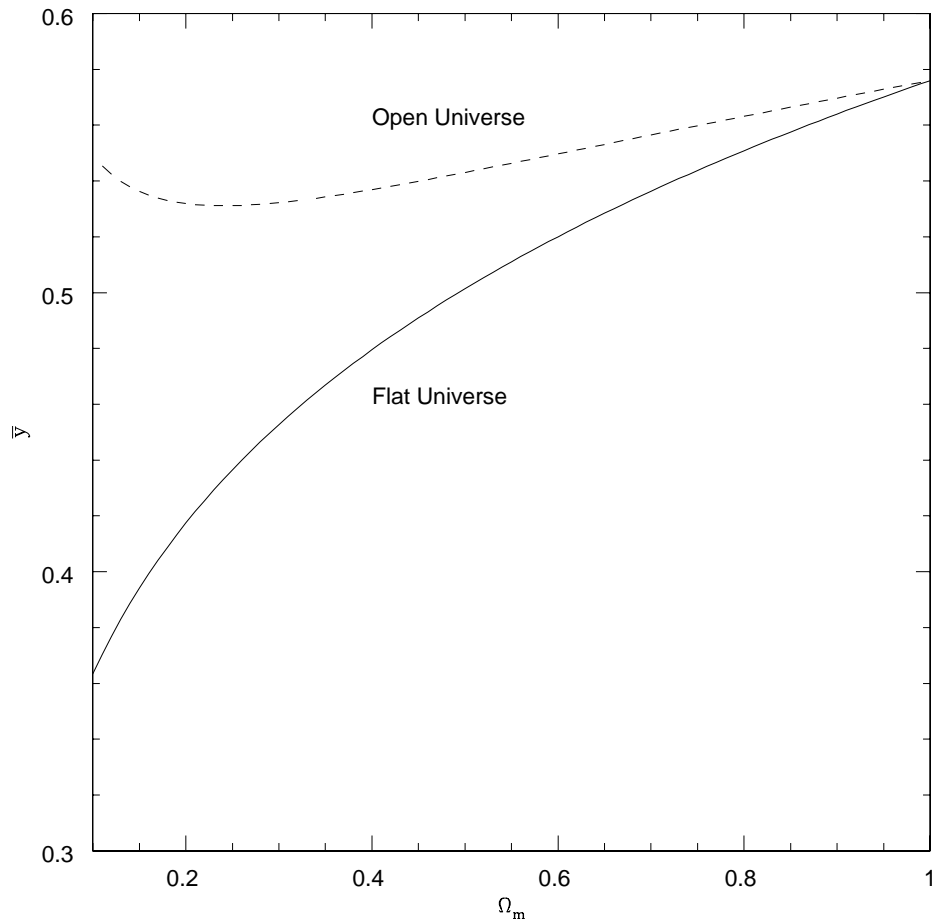


Fig. 3. | Average value of \bar{y} vs. Ω_m for flat and open cosmologies, assuming that energy is conserved.

Fig (3) shows the average value of \bar{y} for different cosmologies, using equations 36 and 51, for $n = 15$.

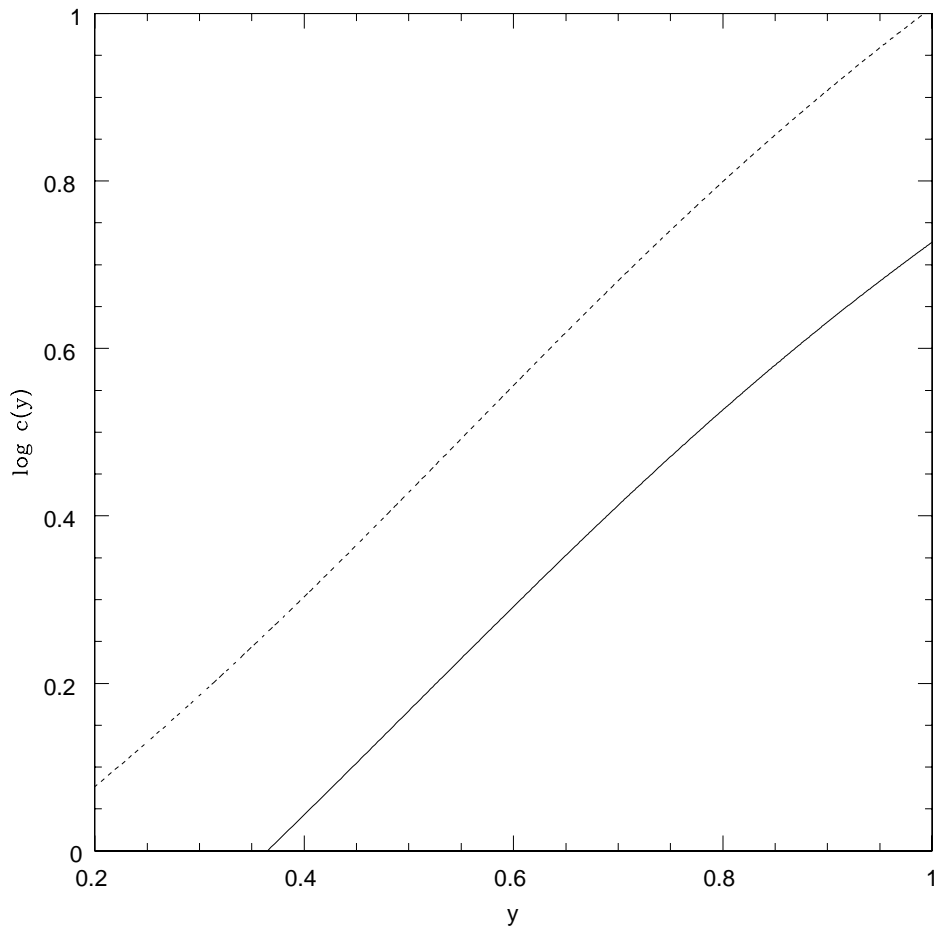


Fig. 4. Concentration parameter vs. y . The solid and dashed curves are for Moore and NFW profiles, respectively.

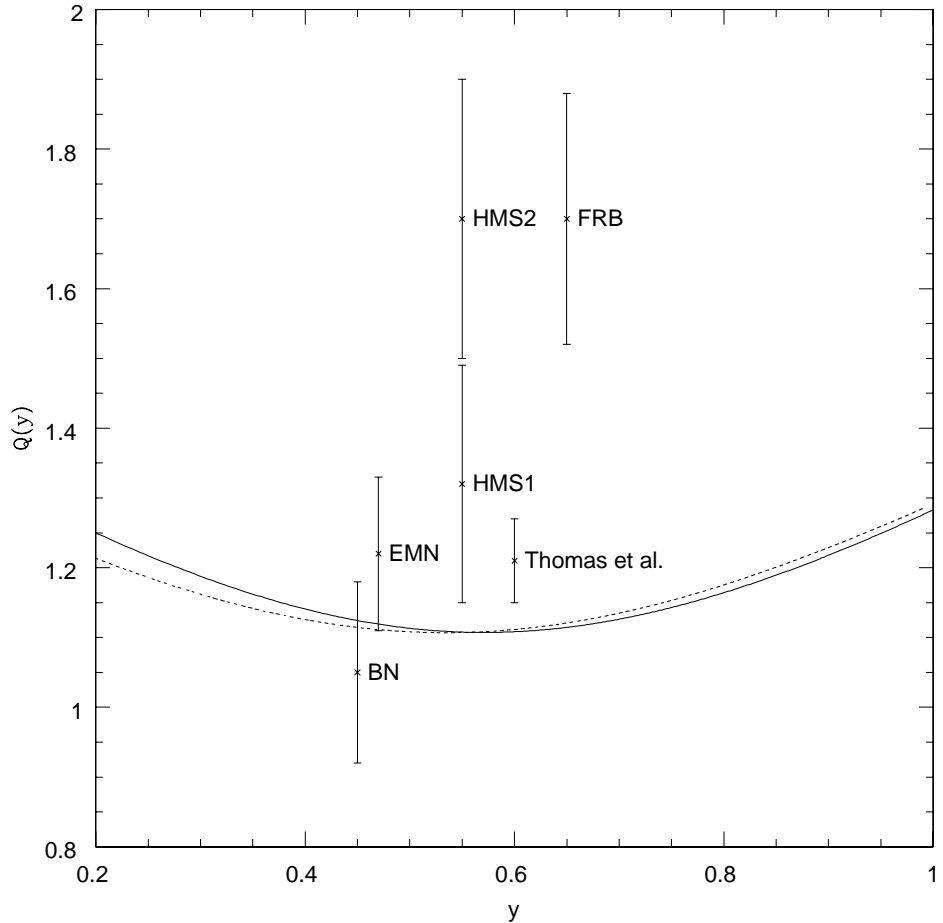


Fig. 5. Normalization Q vs. y , comparison of different results. The solid and dashed curves are for the Moore and NFW profiles respectively. For description of different data points see Table 1. The horizontal position of error bars is arbitrary.

Since all three parameters, $c(f)$, $y(c;f)$ and $Q(c;f)$, are functions of both c and f , one can express any one of them as a function of another, for fixed f . Fig (4) and Fig (5) show concentration parameter c and normalization factor Q as functions of y . The dashed curves are for the NFW profile and the solid curves for the Moore et al. (2000) profile. The x's with error bars show various simulation and observational results (see Table 1). Note

that even if we relax the conservation of energy, one can still use $Q(y)$ or $c(y)$ to find the T - M relation or concentration, using the value y obtained from its definition, equation (49), with the corrected energy.

An important feature of the behavior of $Q(y)$ is the presence of a minimum in or close to the region of physical interest. As a result, $Q(y)$ has very weak dependence on the history of the cluster, for example, the largest variation in Q is about 3%. This is probably why simulations do not show significant cosmology dependence ~ 5% (e.g. EMN, Mathiesen 2000).

Another way of stating this property is that the heat capacity of the cluster is very small. It is well known that the heat capacity of gravitationally bound systems like stars is negative. Yet we know that if non-gravitating gas is bound by an external pressure, its heat capacity is positive. In the case of clusters, the interplay of external accretion pressure and gravitational binding energy causes it to vanish. It is only after the freeze-out time in an extreme open universe (low Ω_m , no cosmological constant) where the heat capacity becomes negative similar to an ordinary gravitationally bound system.

3.5. Concentration Parameter c

As we see in x3.4, concentration parameter is fixed by the cosmology (y parameter) as shown in Fig.(4). This relation can be well fit by:

$$\log_{10} c = 0.17 + 1.2y; \quad (56)$$

for NFW profile, accurate to 5% in the range $0 < y < 1$.

Let us now consider the evolution of c . We know that in an expanding universe Ω_m decreases with time. Comparing with Fig.(4) we see that in a flat CDM universe y is decreasing with time, while in an open/Einstein-de Sitter universe, it is almost constant.

Then equation (56) implies that c is a decreasing function of time (increasing function of redshift) in a CDM universe, while it does not significantly evolve in an OCDM universe. As an example, the concentration parameter in an Einstein-de Sitter universe is about 40% larger than that of a CDM universe with $m = 0.25$. This is consistent with the NFW results who find an increase of about 35% for c as a function of mass in units of non-linear mass scale.

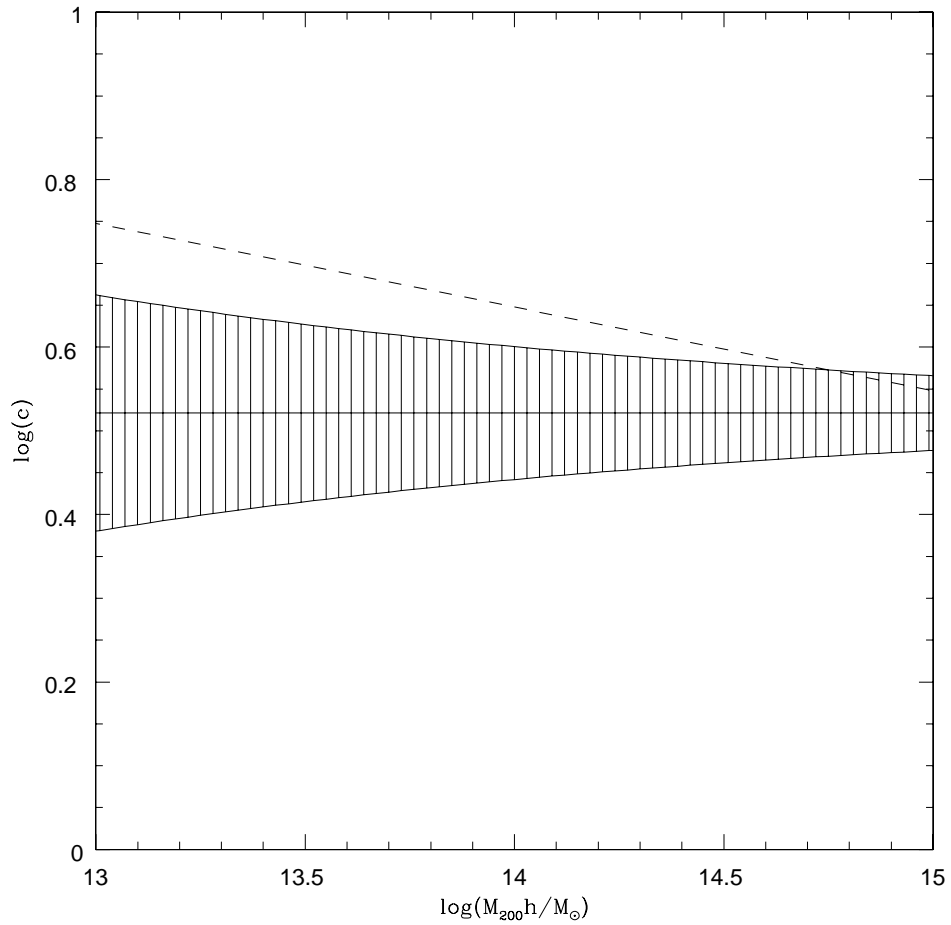


Fig. 6. | Predicted concentration parameter vs. mass for Thomas et al. 2001 simulation. The shaded region indicates the 68% likelihood region. The dashed line is the best fit to their result.

NFW simulations show a weak dependence of the concentration parameter on mass $c / M^{0.1}$. We see that our concentration parameter does not depend on mass. However its scatter is larger for small masses and so is marginally consistent with the simulation results (see Fig 6). Assuming that this discrepancy is only a consequence of non-spherical shape of original proto-cluster, in the next section, we attempt to modify the value of y to match the simulation results.

3.6. Corrections for Initial Non-Sphericity

In this section we try to incorporate the effects due to the non-spherical shape of the initial proto-cluster into our formalism. Unlike previous sections, the calculations of this section are not very rigorous and should be considered as an estimate of the actual corrections. In particular, these approximations lose accuracy if there are large deviations from sphericity which, as we see, is the case for low mass end of the $M-T$ diagram.

We are going to assume that non-sphericity comes in through a modifying factor $1 + N$ that only depends on the initial geometry of the collapsing domain,

$$y_N = y(1 + N); \quad (57)$$

where y_N is the modified value of y . Next, let us assume that $R_i(\theta')$ is the distance of the surface of our collapsing domain from its center. We can expand its deviation from the average in terms of spherical harmonics $Y_m(\theta')$,

$$R_i(\theta') = \sum_m^X a_m Y_m(\theta'); \quad (58)$$

If we try to write down a perturbative expansion for N , the lowest order terms will be quadratic, since there is no rotationally invariant first order term. Moreover, having in mind that the gravitational dynamics is dominated by the large scale structure of the object, as

an approximation, we are going to keep the lowest l value. Since $l=1$ is only a translation of the sphere and does not change its geometry, the lowest non-vanishing multipoles are for $l=2$, and the only rotation invariant expression is

$$N \underset{m=2}{\underset{x^2}{\propto}} a_{2m}^2; \quad (59)$$

where we absorbed any constant factor in the definition of a_{2m} 's. The next simplifying assumption is that a_{2m} 's are Gaussian variables, with amplitudes proportional to the amplitude of the density fluctuations at the cluster mass scale. Mathematically, this is motivated by the fact that the concentration parameter predicted by simulations gets closer to our prediction for spherical proto-clusters, at large mass end, where amplitude gets smaller. The physical motivation is that since the density fluctuations decrease with scale, more massive clusters tend to deviate less from sphericity. Choosing Gaussian statistics for a_{2m} 's is only a simplifying assumption to carry out the calculations. Then it is easy to see that

$$N^{-2} = \frac{6}{25} \langle N \rangle^2; \quad (60)$$

and then using the definition of N , assuming that it is a small correction we get

$$\left(\frac{y_N}{y_N}\right)^2 = \frac{6}{25} \left(1 - \frac{y}{y_N}\right)^2 + \left(\frac{y}{y}\right)^2; \quad (61)$$

Note from equation (51), $y = (H t)^{2/3} (B/A)$ and B/A is given in equation (37). We have also assumed that N and y are statistically independent variables. In the next step, we define the amplitude of N

$$\langle N \rangle = \left(\frac{B}{A}\right)^2; \quad 64 \quad (62)$$

The numerical value of $\langle N \rangle$ is fixed by plugging y_N into equation (56) to get the modified concentration parameter and comparing this result with the simulations of Thomas et al. (Fig 6). Fig 7 shows the modified concentration parameter as a function of mass. We see

that the introduction of non-sphericity results in the cluster concentration parameter being a decreasing function of cluster mass with a scatter that also decreases with mass, in accord with simulations.

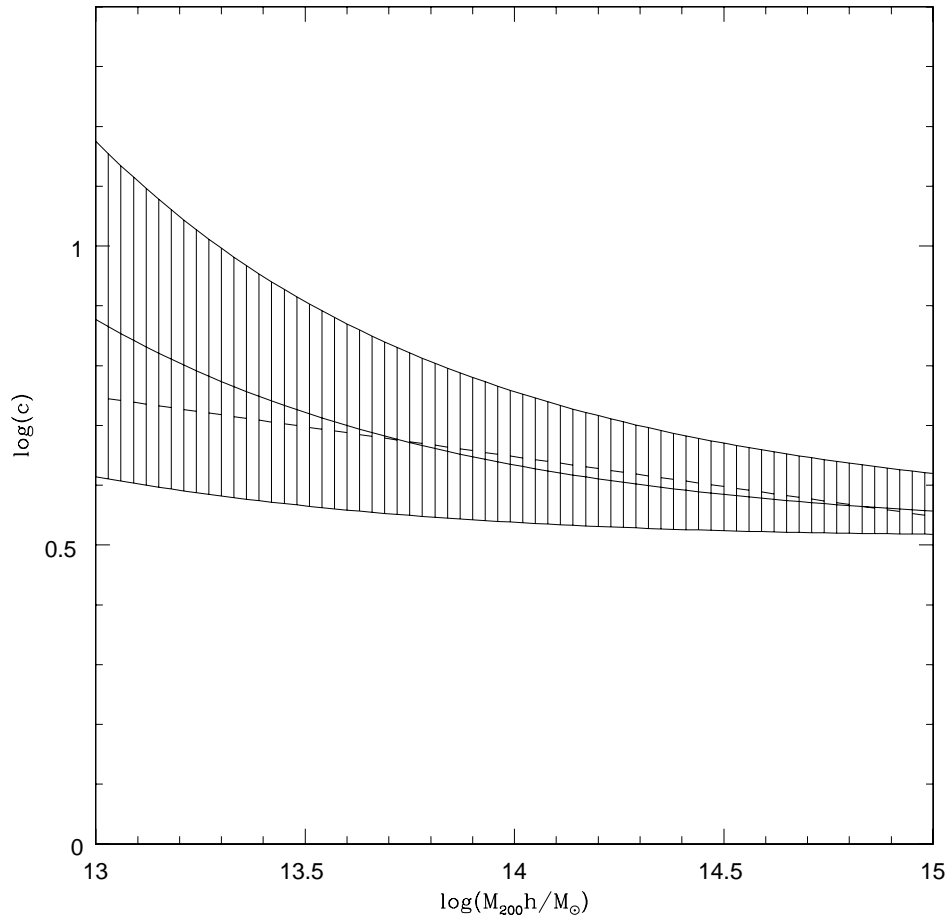


Fig. 7. | Similar to Fig 7 but with non-spherical correction. The solid curve is fitted to match the simulation result.

3.7. Scatter in M -T relation

Since y is linear in $B = A$, it also has a Gaussian probability distribution function (PDF):

$$P(y)dy = \frac{p}{2\pi y^2} \exp\left[-\frac{(y-y_0)^2}{2y^2}\right]; \quad (63)$$

where y and y_0 are related to equations (36) and (37), by equation (51). As we mentioned above, the variation of Q for the average values of y is negligible. However, the scatter in the value of y can be large, specially in the low mass end (see equation 37) and so the scatter in Q might become significant. In what follows we only consider the NFW profile, since it is extensively considered in the literature. We find that the behavior of Q can be fitted by:

$$Q(y)^2 = Q_0^2 + N(y - y_0)^2; \quad (64)$$

where

$$Q_0 = 1.11; N = 1.8; y_0 = 0.538; \quad (65)$$

The error in this fitting formula is less than 3% in the range $1 < y < 2$. Inserting this into equation (63) leads to the PDF of Q :

$$P(Q)dQ = \frac{p}{2\pi y^2 N (Q^2 - Q_0^2)} \exp\left[-\frac{(y_0 - y)^2 + (Q^2 - Q_0^2)N}{2y^2}\right] \cosh\left[\frac{y_0 - y}{y}\right] \frac{Q}{N} \frac{2QdQ}{(Q^2 - Q_0^2)}; \quad (66)$$

Fig 8 shows three different examples of the PDF obtained here. It is clear that the scatter in Q is asymmetric. In fact, since the average value of y is close to the minimum of equation (57), the scatter in y shifts the average value of Q upwards systematically. In the limit of large y , where this shift is significant, $P(Q)$ is approximately:

$$P(Q)dQ = \frac{p}{2\pi y^2 N (Q^2 - Q_0^2)} \exp\left[-\frac{(Q^2 - Q_0^2)}{2N y^2}\right] H(Q - Q_0); \quad (67)$$

where H is the Heaviside step function.

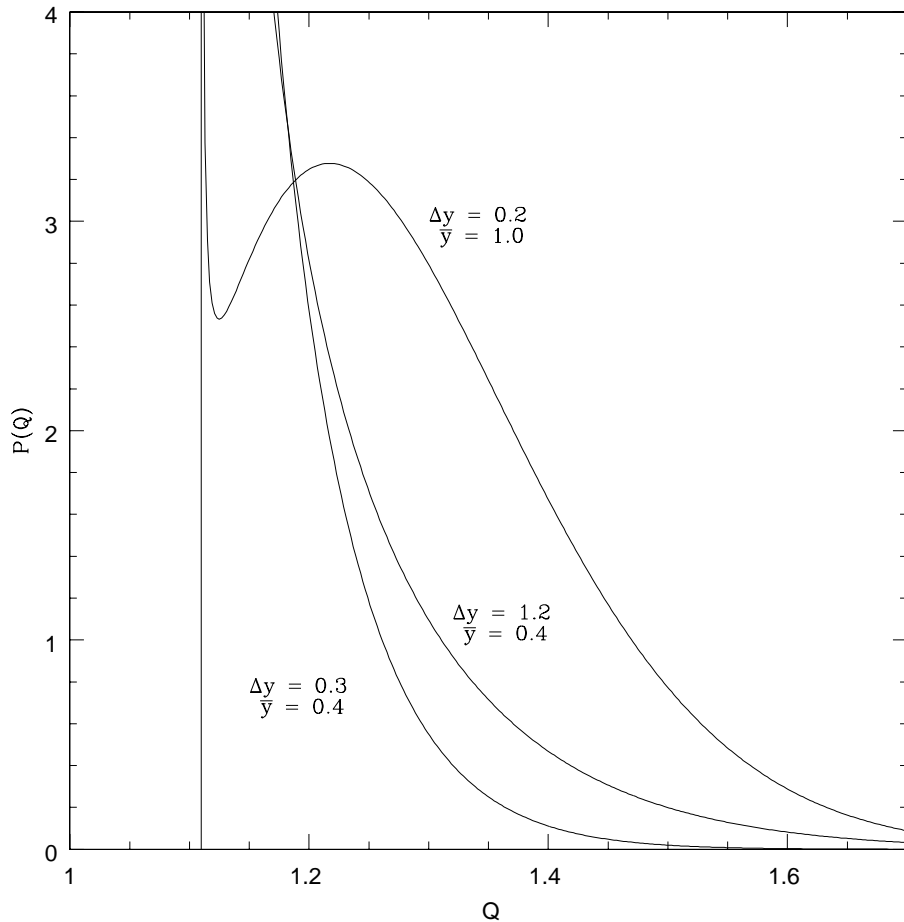


Fig. 8. | Probability distribution function of normalization for three different y and \bar{y} 's. The PDF vanishes for $Q < Q_0 = 1.11$. The large value of $y = 1.0$ is possible if one includes non-spherical corrections (x3.6).

Although the assumption of Gaussianity is not strictly valid for y_N which includes non-spherical corrections, we still can, as an approximation, use the above expressions for the PDF by replacing y and \bar{y} by y_N and \bar{y}_N . It is also easy to find the average of Q^2

$$\langle Q^2 \rangle = Q_0^2 + N [(y - y_0)^2 + \bar{y}^2]:$$

As an example, for $y = y_0$, while $y = 0.5$ gives only about 16% systematic increase in Q , $y = 1.0$ leads to 60% increase.

3.8. Observed and Average Temperatures

The temperature found in x2.4 is the density weighted temperature of the cluster averaged over the entire cluster. However, the observed temperature, T_f , can be considered as a flux-weighted spectral temperature averaged over a smaller, central region of the cluster. The two temperatures may be different, due to presence of inhomogeneities in temperature. We use the simulation results by Mathiesen & Evrard (2001) to relate these two temperatures and refer the reader to their paper for their exact definitions and the discussion of the effects which lead to this difference:

$$T = T_f [1 + (0.22 \pm 0.05) \log_{10} T_f (\text{keV}) \pm (0.11 \pm 0.03)] \quad (68)$$

This correction changes the mass-temperature relation from $M \propto T^{1.5}$ to $M \propto T^{1.64}$ for the observed X-ray temperatures. We use this correction in converting the observed X-ray temperature to virial temperature in Figures 1 and 9–11.

4. Predictions vs. Observations

4.1. Power Index

It is clear from equation (54) that we arrive at the usual $M \propto T^{1.5}$ relation that is expected from simple scaling arguments and is consistent with the numerical simulations (e.g. EMN or Bryan and Norman 1998). On the other hand, the observational model mass estimates lead to a steeper power index in the range 1.7–1.8. Although originally interpreted as an artifact of the model (HMS), the same behavior was seen for masses

estimated from resolved temperature profile (FRB). FRB carefully analyzed the data and interpret this behavior as a bend in the $M-T$ at low temperatures. This was confirmed by Xu, Jin & Wu (2001) who found the break at $T_X = 3-4$ keV.

As discussed in x3.7, the asymmetric scatter in Q introduces a systematic shift in the $M-T$ relation. For large values of y all of the temperatures are larger than the value given by the scaling relation (54) for average value of y . This scatter increases for smaller masses (see equation 37), hence smaller clusters are hotter than the scaling prediction. As a result, the $M-T$ relation becomes steeper in the low mass range as Q increases, while the intrinsic scatter of the data is also getting larger. Indeed, increased scatter is also observed in the FRB data (Fig 1 and Fig's 9-11 to compare with our prediction) but they interpret it as the effect of different formation redshifts. We will address this interpretation in x5.

4.2. Normalization

As we discussed in x3.4, our normalization (i.e., Q in equation 55) is rather stable with respect to variations of cosmology and the equilibrium density profile. Table 1 compares this value with various observational and simulation results.

Q	Method	Reference
1.12 0.02	Analytic	This paper
1.21 0.06	Hydro-Simulation	Thom as et al. 2001
1.05 0.13	Hydro-Simulation	Bryan & Norman 1998 (BN)
1.22 0.11	Hydro-Simulation	Evrard et al. 1996 (EMN)
1.32 0.17	Optical mass estimate	Homer et al. 1999 (HMS1)
1.70 0.20	Resolved temperature profile	Homer et al. 1999 (HMS2)
1.70 0.18	Resolved temperature profile	Finoguenov et al. 2001 (FRB)

Table 1. Comparison of normalizations from different methods. The last two rows only include clusters hotter than 3 keV.

We see that our analytical method is consistent with the hydro-simulation results, indicating validity of our method, since both have a similar physics input and the value of α_{spec} used here was obtained from simulations. On the other hand, X-ray mass estimates lead to normalizations about 50% higher than our result and simulations. The result of the optical mass estimates quoted is marginally consistent with our result.

Assuming that this is true would imply that optical masses are systematically higher than X-ray masses by ~80%. Aron et al. (1999) have compared optical and X-ray masses for a sample of 14 clusters and found, on the contrary, a systematic difference less than 10%. The optical masses used in the work of Aron et al. (1999) were all derived by CNOOC group (Carlberg et al. 1996) while the Girardi et al. 1998 data, used in HMs analysis quoted above, was compiled from different sources and has larger scatter and unknown systematic errors. In fact HMs excluded a number of outliers to get the correct slope and original data had even larger scatter (see their Fig 1). Therefore it may be that the systematic error in the optical result of Table 1, is much larger and so in agreement with other observations.

As discussed in x3.1, one possible source for difference between theoretical and observational normalizations is that the values for α_{spec} are different in the two cases due to systematic selection effects. Also, intriguingly, Bryan & Norman (1998) show that there is a systematic increase in the obtained value of α_{spec} by increasing the resolution of the simulations. Whether this is a significant and/or real effect for even higher resolutions is not clear to us.

However, the fact that the slope is unchanged indicates that the missing process is, probably, happening at small scales and so relates the intermediate-scale temperature to

the small-scale flux-weighted spectral temperature by a constant factor, independent of the large-scale structure of the cluster. In this case the actual value of ϵ_{spec} must be 0.6.

Figures 9–11 show the prediction of our model, shifted downwards to fit the observational data in the massive end, versus the observational data of FRB using resolved temperature profile and corrected as discussed in §3.8. The correction due to initial non-sphericity (§3.6) is included in the theoretical plot. The value of β which enters $B = A$ (equation 37) through M_{OL} , is fixed by cluster abundance observations (e.g. Bahcall & Fan 1998).

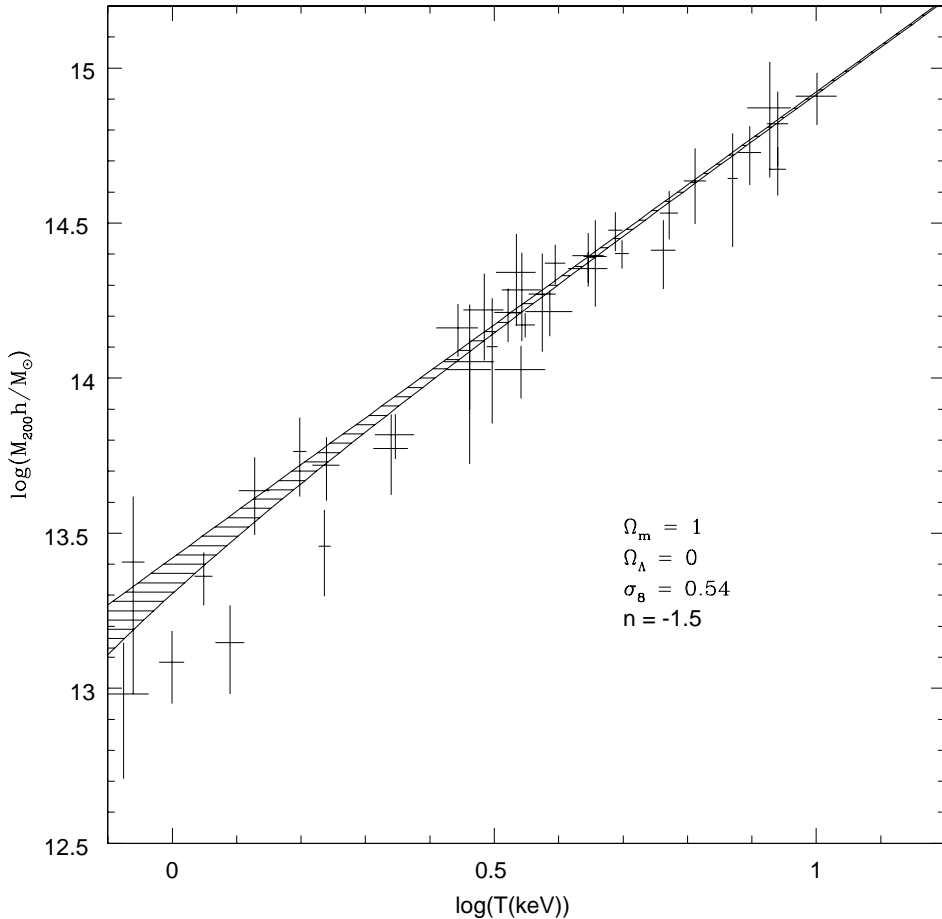


Fig. 9. Our result with shifted normalization for an Einstein-de Sitter universe vs. FRB data. The shaded area indicates the 68% confidence level region (x3.7).

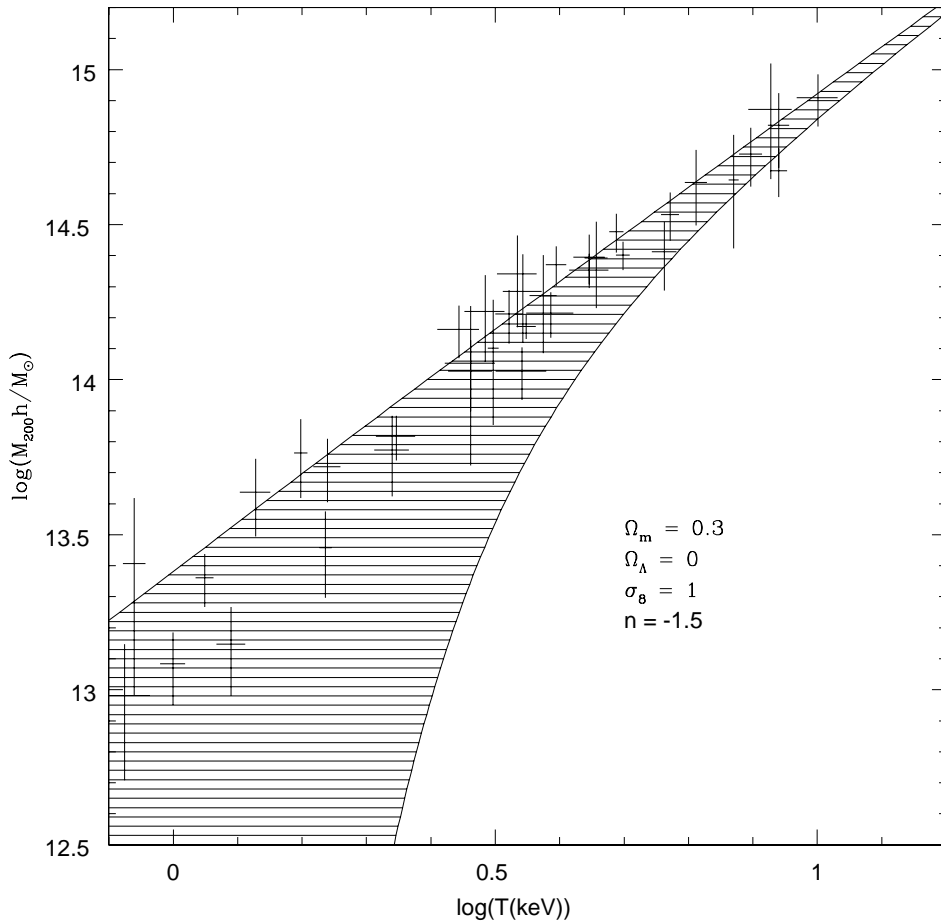


Fig. 10. | Our result with shifted normalization for an Λ CDM universe vs. FRB data. The shaded area indicates the 68% confidence level region ($\times 3.7$).

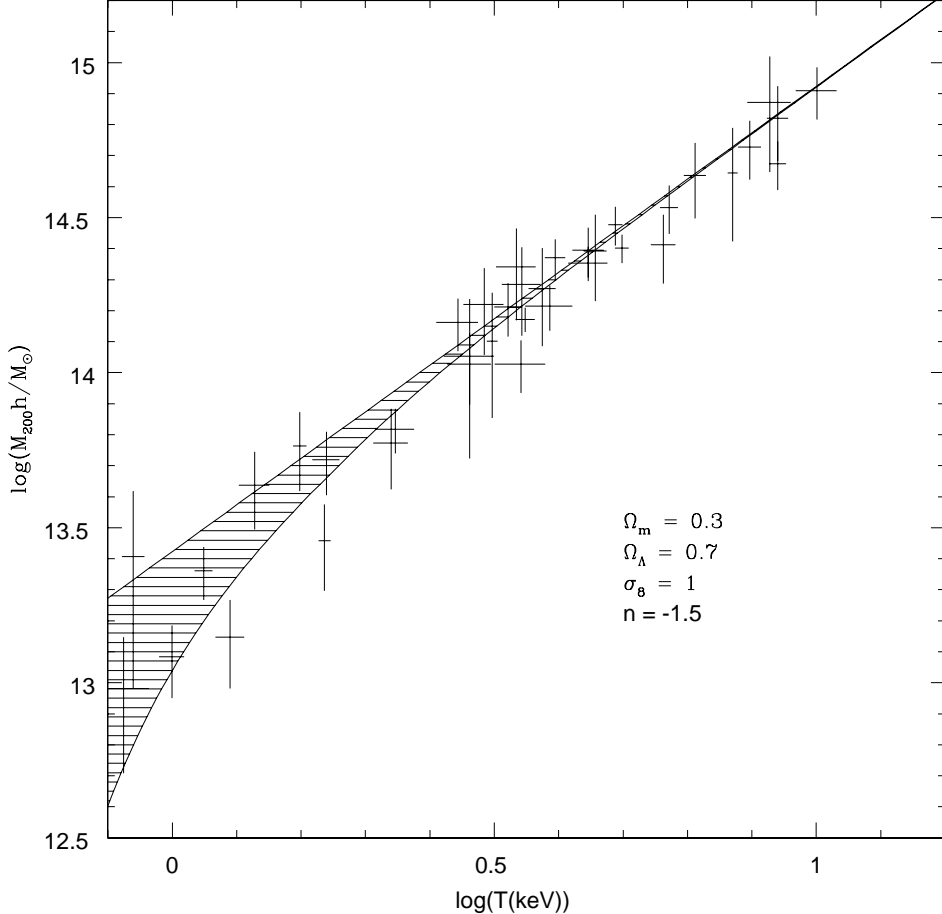


Fig. 11. | Our result with shifted normalization for a CDM universe vs. FRB data. The shaded area indicates the 68% confidence level region (x3.7).

We see that while an Einstein-de Sitter cosmology underestimates the scatter in the low mass end, a typical low density OCDM cosmology overestimates it. On the other hand, a typical CDM cosmology is consistent with the observed scatter. Interestingly, this is consistent with various other methods, in particular CMB + SNeIa (ref.) result which point to a low-density universe.

4.3. Evolution of M-T Relation

As we discussed in x3.4, the value of our normalization has a weak dependence on cosmology. Going back to equation (54), we see that the time dependence of the M-T relation is simply: $M \propto H^{-1} T^{1.5}$. Assuming a constant value of $\tilde{\gamma}_{\text{spec}}$, this formula can be potentially used to measure the value of H at high redshifts and so constrain the cosmology.

Schindler (1999) has compiled a sample of 11 high redshift clusters ($0.3 < z < 1.1$) from the literature with measured isothermal model masses. In these estimates, the gas is assumed to be isothermal and have the density profile:

$$\rho(r) = \rho_0 (1 + (\frac{r}{r_c})^2)^{-3/2} \quad (69)$$

Then, the mass in overdensity δ_c is given by:

$$M \propto (\frac{3H^2}{2G})^{1/2} (\frac{3\pi r_c^3 k T}{G m_p})^{3/2} \quad (70)$$

Comparing this with equation (54), and neglecting the difference between virial and X-ray temperatures, we get:

$$Q \propto (3)^{2/3} (\tilde{\gamma}_{\text{spec}})^{1/3} \quad (71)$$

In the last two equations, we have ignored r_c with respect to the radius of the virialized region, which introduces less than 3% error. So we can find the normalization Q from the value of $\tilde{\gamma}_{\text{fit}}$ (independent of cosmology in this case).

Assuming $\tilde{\gamma}_{\text{spec}} = 0.9$, equation (71) gives the value of Q for a given $\tilde{\gamma}_{\text{fit}}$. Fig 12 shows the value of Q versus redshift for Schindler (1999) sample and also FRB resolved temperature method for low redshift clusters. This result is consistent with no redshift dependence and the best fit is:

$$\log Q = 0.23 - 0.01(\text{systematic}) - 0.04(\text{random}) + (0.09 - 0.04)z \quad (72)$$

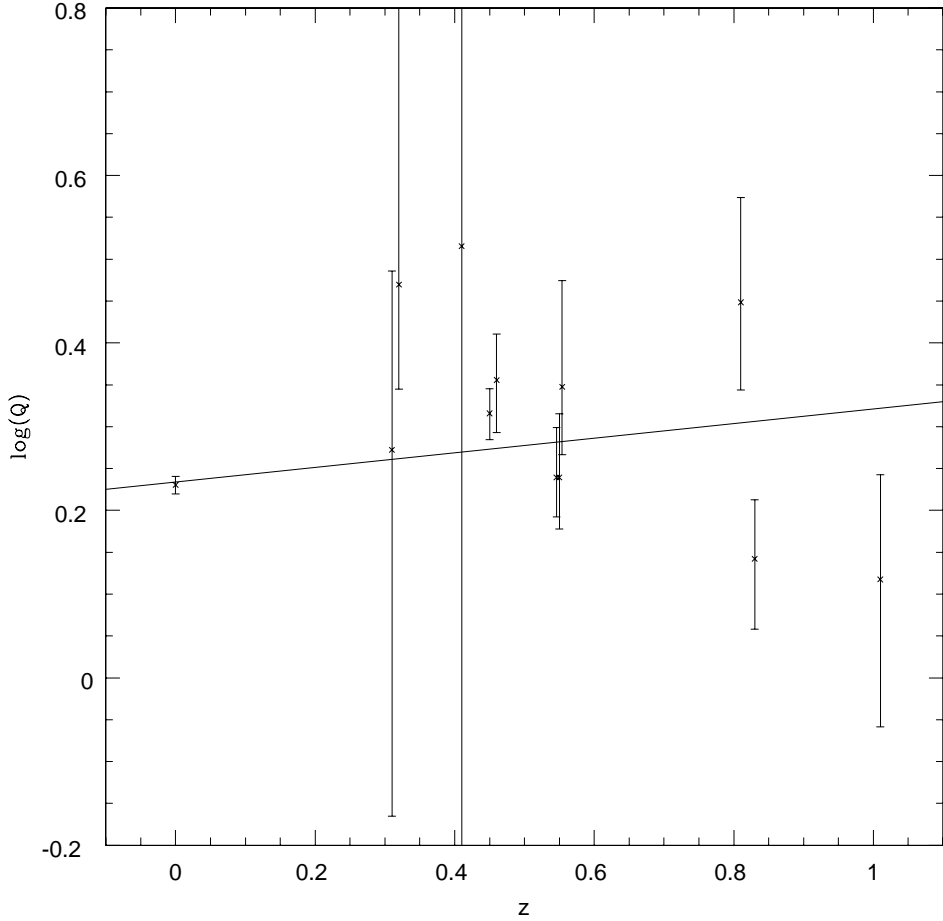


Fig. 12.| Evolution of the normalization Q with redshift. The data points are from Schindler (1999) high- z sample and FRB low- z normalization at $z = 0$. The line is the best fit.

The combination of this result and equation (55) gives

$$kT = (11.24 \text{ keV}) e^{0.21z} \left(\frac{M}{10^{15} h^{-1} M_{\odot}} \right)^{2/3} \quad (73)$$

which relates X-ray temperature of galaxy clusters to their masses that does not depend on the theoretical uncertainties with regard to the normalization coefficient of the M-T

relation, in this range of redshifts. The systematic error in this result is less than 5% while the random scatter can be as large as 20%. This result is valid for $T_x > 4 \text{ keV}$ since below this temperature the systematic shift due to random scatter becomes significant (x3.7). It is easy to see that this threshold moves to lower temperatures in high redshifts in our formalism.

Note that the more realistic interpretation of a possible evolution in observed Q , obtained above, is that in equation (71), Q remains constant (Fig 5) and, instead, $\tilde{\gamma}_{\text{spec}}$ varies with time. However there will be no difference at the level of the M - T relation and, moreover, the weak redshift dependence in equation (73) shows that $\tilde{\gamma}_{\text{spec}}$ is indeed almost constant.

5. Discussion

In this section we discuss the validity of different approximations which were adopted throughout this paper.

In the calculation of initial and final energy of the cluster, we ignored any contribution from the vacuum energy. In fact we know that cosmological constant in the Newtonian limit can be considered as ordinary matter with a constant density. If the cosmological constant does not change with time, then its effect can be considered as a conservative force and so energy is conserved. However, in both initial state and final equilibrium state of the cluster the density of cosmological constant is much smaller than the density of matter and hence its contribution is negligible. This does not hold for quintessential models of the vacuum energy since it changes with time and energy is not conserved. This may be used as a potential method to distinguish these models from a simple cosmological constant.

Let us make a simple estimate of the importance of this effect. We expect the relative

contribution of a varying cosmological constant be maximum when the density of the proto-cluster is minimum. This happens at the turn-over radius which is almost twice r_v , the virial radius, in the top-hat approximation. Then the contribution to the energy due to the vacuum energy would be:

$$\frac{E}{E} \quad \left(\frac{4}{3} (t_0=2) (2r_v)^3 \right) M = \left(\frac{8}{200} \right) \left(\frac{(t_0=2)}{c(t_0)} \right) = \left(\frac{8}{200} \right) \left(\frac{H^2(t_0=2)}{H^2(t_0)} \right) \quad (t_0=2) \quad 0:1: \quad (74)$$

This gives about 10% correction to y or about 15% correction to c . We see that still the effect is small but, in principle observable if we have a large sample of clusters with measured concentration parameters.

A systematic error in our results might have been introduced by replacing the density distribution by an averaged radial profile which underestimates the magnitude of gravitational energy and so the temperature. Also, as shown by Thomas et al. (2000), most of the clusters in simulations are either steeper or shallower than the NFW profile at large radii. Since our normalization is consistent with simulation results, we think that these effects do not significantly alter our predictions.

Let us now compare our results with that of Voit (2000), who made the first such analytic calculation (but we were not aware of his elegant work until the current work was near completion) and uses the same ingredients to obtain $M-T$ relation. First of all, as noted in x3.3, his result, which is equivalent to the central peak approximation to find $B=A$, ignores the possibility of mergers. As we see in Fig (2) the value of $B=A$ and so y is about 50% larger in the single peak case than the multiple peak case. Although it does not change the normalization very much, it overestimates the concentration parameter, in a way which is even more inconsistent with the simulation results (it refers to $\log c = 0.8$ in Fig 6). Moreover, neglecting the cosmology dependence of the surface correction, $\frac{1+}{1}$, gives a false cosmology dependence to the normalization (Fig 3 in Voit 2000), which is inconsistent with hydro-simulations (e.g. EMN, Matherne 2000) and does not give the systematic shift

in the lower mass end.

Finally, we comment on the interpretation of the scatter/bent in the lower mass end as being merely due to different formation redshifts which is suggested by FRB. Although different formation redshifts can certainly produce this scatter/bent, it is not possible to distinguish it from scatter in initial energy of the cluster or its initial non-sphericity, in our formalism. On the other hand, the FRB prescription, which assumes constant temperature after the formation time, is not strictly true because of the on-going accretion of matter even after the cluster is formed. So, as argued by Mathiesen 2000 using simulation results, the formation time might not be an important factor while the same effect is produced by scatter in initial conditions of the proto-cluster.

6. Conclusion

We combine conservation of energy with the virial theorem to constrain the mass-temperature relation of the clusters of galaxies and obtain the following results:

Considering the scatter in the lower mass end, our slope is consistent with that of simulations and observations.

Our normalization is consistent with numerical hydro-simulations and about 50% higher than the X-ray mass estimate results. This is probably due to our poor understanding of the history of the cluster gas. Our normalization is marginally consistent with the optical mass-estimate results, but this is probably because the latter has a large systematic error.

Our normalization has a very weak dependence on cosmology and formation history. This is consistent with simulation results.

We can reproduce the recently observed scatter/bent in the M-T relation in the lower mass end for a low density CDM cosmology, while Einstein-de Sitter/OC DM cosmologies under/overestimate this scatter/bent. We conclude that the behavior at the low mass end of the M-T diagram can be used to constrain cosmological models.

We can determine the concentration parameter of the cluster and its scatter. This is marginally consistent with simulation results. In fact, we can find non-spherical corrections to M-T relation by fitting our concentration parameter to the simulation results.

We find mass-temperature relation (73), for clusters of galaxies, based on the observations calibrated by our formalism, which can be used to find masses of galaxy clusters from their X-ray temperature in the range of redshift $0 < z < 1.1$ with the accuracy of 20%. This is a powerful tool to find the evolution of mass function of clusters, using their temperature function.

This research is supported in part by grants NAG 5-8365. N.A. wishes to thank Ian dell'Antonio, Licia Verde and Eiichiro Komatsu for useful discussions.

R E F E R E N C E S

Aaron, L D ., Ellingson, E ., Morris, S L ., Carlberg, R G . 1999, ApJ, 517, 2, 587

Bahcall, N A ., & Cen, R . 1992, ApJ, 398, L81

Bahcall, N A ., Fan, X ., & Cen, R . 1997, ApJ, 485, L53

Bahcall, N A ., & Fan, X . 1998, ApJ, 504, 1

Bialek, J.J., Evrard, A E ., Mohr, J.J., astro-ph/0010584

Banton, M ., Cen, R ., Ostriker, J P ., Strauss, M A ., & Tegmark, M . 2000, ApJ, 531, 1

Bryan, G L ., & Norman, M L . 1998, ApJ, 495, 80

Bryan, G L ., astro-ph/0009286

Carlberg, R G . et al. 1996, ApJ, 462, 32

Eke, V R ., Cole, S ., & Frenk, C S . 1996, MNRAS, 282, 263

Evrard, A E ., Metzler, C A ., & Navarro, J F . 1996, ApJ, 469, 494 (EMN)

Finoguenov, A ., Reiprich, T . H ., & Böhringer, H ., astro-ph/0010190 (FRB)

Giardini, M ., Giuricin, G ., Mardirossian, F ., Mazzetti, M ., Boschin, W . 1998, ApJ, 505, 74

Giardini, M ., Mazzetti, M . 2000, ApJ, 548, 79

Gunn, J., Gott, J. 1972, 176, 1

Henry, J P . 2000, ApJ, 565, 580

Hjorth, J., Oukbir, J. & van Kampen, E . 1998, MNRAS, 298, L1

Homer, D J ., Moshotzky, R F ., & Scharf, C A . 1999, ApJ, 520, 78 (HMS)

Matheriesen, B F ., astro-ph/0012117

Matheriesen, B F ., Evrard, A E . 2001, ApJ 546, 1, 100

Muanwong et al., astro-ph/0102048

Navarro, Frenk & White 1997, ApJ 490, 493 (NFW)

Nevalainen, J., Markovitch, M., & Forman, W. 2000, ApJ, 532, 694

Neumann, D. M., & Arnaud, M. 1999, A & A, 348, 711

Oukbir, J., Bartlett, J.G., & Blandford, R. 1997, A & A, 320, 365

Padmanabhan, T., Structure Formation in the Universe, 1993, Cambridge University Press

Peebles, P.J.E., Daly, R.A., & Juszkiewicz, R. 1989, ApJ, 347, 563

Pen, U. 1998, ApJ, 498, 60

Schindler, S. 1999, A & A, 349, 435

Thomas, P.A. et al., astro-ph/0007348

Tyson, J.A., Kochanski, G.P., & dell'Antonio, I.P. 1998, ApJ, 498, L107

Voit, M. 2000, ApJ 543, 1, 113

Viana, P.T.P., & Liddle, A.R. 1996, MNRAS, 281, 323

White, S.D.M., Efstathiou, G., & Frenk, C.S. 1993, MNRAS, 262, 102

Xu, H., Jin, G., Xiang-Ping, W., astro-ph/0101564

A. Statistics of $b=a$

a and b are defined as:

$$a = \int_0^1 i(x) d^3x; b = \int_0^1 (1 - x^2) i(x) d^3x \quad (A1)$$

Assuming a Gaussian statistics for the linear density field, The Probability Distribution Function for a and b , takes a Gaussian form :

$$\begin{aligned} P(a; b) da db &= \frac{1}{2\pi L} \exp \left[-\frac{1}{2L} (\langle b^2 \rangle - \langle a^2 \rangle - \langle ab \rangle^2) \right] da db; \\ L &= \langle a^2 \rangle \langle b^2 \rangle - \langle ab \rangle^2 : \end{aligned} \quad (\text{A } 2)$$

Then, for fixed a , we have:

$$\frac{\langle b \rangle}{a} = \frac{\langle ab \rangle}{\sqrt{\langle a^2 \rangle}} \quad (\text{A } 3)$$

$$b = \frac{L}{\sqrt{\langle a^2 \rangle}} : \quad (\text{A } 4)$$

To find the quadratic moments of a and b , we assume a power-law linear correlation function:

$$\langle_i(r) = \langle_i(x) \langle_i(x + r) \rangle = \left(\frac{r_{0i}}{r}\right)^{3+n} : \quad (\text{A } 5)$$

The moments become:

$$\langle a^2 \rangle = 8^2 \left(\frac{r_{0i}}{R_i}\right)^{3+n} F_{00}(n); \quad (\text{A } 6)$$

$$\langle ab \rangle = 8^2 \left(\frac{r_{0i}}{R_i}\right)^{3+n} (F_{00}(n) - F_{02}(n)); \quad (\text{A } 7)$$

$$\langle b^2 \rangle = 8^2 \left(\frac{r_{0i}}{R_i}\right)^{3+n} (F_{00}(n) - 2F_{02}(n) + F_{22}(n)); \quad (\text{A } 8)$$

where $F_{m1}(n)$ is defined as:

$$F_{m1}(n) = \frac{1}{8} \int_0^{\pi} \int_0^{\pi} \int_0^{\pi} x_1^m x_2^1 j_{x_1} x_2 j^{(n+3)} d^3 x_1 d^3 x_2; \quad (\text{A } 9)$$

where the integral is taken inside the unit sphere. Taking the angular parts of the integral, this reduces to:

$$F_{m1} = \frac{1}{n+1} \int_0^{\pi} \int_0^{\pi} dx_1 dx_2 x_1^{m+1} x_2^{1+n} (j_{x_1} x_2 j^{1-n} - j_{x_1} + x_2 j^{1-n}): \quad (\text{A } 10)$$

{ 46 }

Then, taking this integral for the relevant values of m and l , and inserting the result into (A 6-A 8) and subsequently (A 3-A 4) gives:

$$\frac{\langle b \rangle}{a} = \frac{4(1-n)}{(n-5)(n-2)}; \quad (A 11)$$

with

$$b = \frac{16 \cdot 2^{n-2}}{(5-n)(2-n)} \left[\frac{n+3}{n(7-n)(n-3)} \right]^{\frac{1}{2}} \left(\frac{r_{0i}}{R_i} \right)^{\frac{n+3}{2}}; \quad (A 12)$$